


## Research Article

# Numerical Performance Investigation of Parabolic Dish Solar-Assisted Cogeneration Plant Using Different Heat Transfer Fluids

Muhammad Sajid Khan,<sup>1,2</sup> Muhammad Abid,<sup>3</sup> Khuram Pervez Amber,<sup>2</sup>  
Hafiz Muhammad Ali ,<sup>4</sup> Mi Yan,<sup>1</sup> and Samina Javed<sup>5</sup>

<sup>1</sup>Institute of Energy and Power Engineering, Zhejiang University of Technology, Hangzhou, Zhejiang 310014, China

<sup>2</sup>Department of Mechanical Engineering, Mirpur University of Science and Technology (MUST), Mirpur 10250 (AJK), Pakistan

<sup>3</sup>Department of Energy Systems Engineering, Faculty of Integrated Technologies, Universiti Brunei Darussalam, Jalan Tungku Link BE 1410, Bandar Seri Begawan, Brunei Darussalam

<sup>4</sup>Mechanical Engineering Department, King Fahd University of Petroleum & Minerals (KFUPM), Dhahran 31261, Saudi Arabia

<sup>5</sup>Department of Mechanical Engineering, University of Engineering and Technology, Taxila 47050, Pakistan

Correspondence should be addressed to Hafiz Muhammad Ali; [hafiz.ali@kfupm.edu.sa](mailto:hafiz.ali@kfupm.edu.sa)

Received 6 February 2021; Revised 27 March 2021; Accepted 13 April 2021; Published 28 April 2021

Academic Editor: Regina De Fátima Peralta Muniz Moreira

Copyright © 2021 Muhammad Sajid Khan et al. This is an open access article distributed under the Creative Commons Attribution License, which permits unrestricted use, distribution, and reproduction in any medium, provided the original work is properly cited.

Parabolic dish solar collectors gain higher solar to thermal conversion efficiency due to their maximum concentration ratio. The present research focuses by integrating the parabolic dish solar collector to the steam cycle producing power and rate of process heating. Pressurized water, therminol VP1, and supercritical carbon dioxide are the examined working fluids in the parabolic dish solar collector. The aim of the current research is to observe the optimal operating conditions for each heat transfer fluid by varying inlet temperature and flow rate of the working fluid in the parabolic dish solar collector, and combination of these parameters is predicted to lead to the maximum energy and exergy efficiencies of the collector. The operating parameters are varied to investigate the overall system efficiencies, work output, and process heating rate. Findings of the study declare that water is an efficient heat transfer fluid at low temperature levels, whereas therminol VP1 is effective for a higher temperature range. The integrated system efficiencies are higher at maximum flow rates and low inlet temperatures. The efficiency map of solar collector is located at the end of study, and it shows that maximum exergy efficiency gains at inlet temperature of 750 K and it is observed to be 37.75%.

## 1. Introduction

Renewable energy resources are considered the best alternative solutions to address the severe ecological problems created due to the consumption of fossil fuels [1]. Although there are various types of renewable energy resources (geothermal, solar, and wind etc.), solar energy is a unique choice as it is available abundantly [2]. Concentrating solar systems, also known as concentrated solar power (CSP) technologies, gain more interest due to their useful heat production at elevated temperatures. Particularly, dish solar collectors are an efficient source that converts solar energy into useful thermal energy and also attain maximum thermal efficiency due to higher concentration ratio [3]. Its operation relies on the

concentration of solar radiations onto a small receiver where it exchanges heat with the working fluid. The application of the cavity receiver has been noticed to be a very useful technique as solar radiations are properly centered on parabolic solar dishes [4]. The useful heat gain from solar dish collectors can be used as an input source for dryers, hydrogen production systems, and Rankine and Brayton cycles [5, 6].

The literature consists of both numerical and experimental works regarding parabolic dish cavity receivers. Daabo et al. [7] performed numerical analysis of various parabolic dish cavity receivers to investigate their optical performance. Results indicated that the conical shaped receiver received and absorbed maximum solar radiations per unit area as compared to the others with optical efficiency near to

75.3%. The optimization of the receiver employing optimal methods and CFDs was conducted to examine the most suitable position of the solar receiver on a concentrator collector by Przenzak et al. [8]. The optimized value of fluid flow was calculated to be 0.6 m/s without any overheating of the receiver body, and it also decreased the convection and radiation heat losses. Jilte et al. [9] investigated the dish collector with different cavity shapes mathematically, and research was performed for five inclinations and three different isothermal wall temperatures. The conical cavity receiver showed the lowest convective heat losses as compared to the other investigated receivers. Kaushika and Reddy [10] suggested a method for design and development of a low-cost steam generation system integrated with a parabolic dish (PD) system. Solar to steam conversion efficiency was found to be 70 to 80% at 723 K. Parabolic dish using cavity receiver was numerically modeled and thermally optimized by Loni et al. [11].

Experimental work has been performed to analyze the energetic and exergetic performances of the SK-14 cylindrical cavity solar dish system [12]. Heat loss factor was observed to be 4.6 W/K with 52% optical efficiency under higher solar insulations. Mohammad [13] designed and developed a parabolic dish solar (PDS) water heater for domestic usage. Thermal efficiencies were between 52% and 56% that showed the reliability of the designed system. Reddy et al. [14] carried out an experimental work on a 20 m<sup>2</sup> prototype fuzzy focal dish receiver. Madadi et al. [15] theoretically and experimentally analyzed the energetic and exergetic performances of PDSC. Two different cavity receivers, namely, cylindrical and conical, were taken into account with different parameters. It was observed that almost 35% to 60% of the exergy destroyed was due to the heat transfer from the sun to the receiver. The cylindrical cavity receiver showed better results than the counterpart did.

Furthermore, utilization of heat transfer fluid (HTF) has an immense impact on the efficiency of solar collectors. The most used HTFs in concentrated solar power (CSP) technologies are oil-based, while molten salts are also tested by researchers [16, 17]. Loni et al. [18] conducted a study using different cavity receivers of PDC utilizing water and Behran oil as heat transfer fluids. Another study was conducted by Loni et al. [19] using air as a HTF in a dish collector integrated with organic Rankine cycle (ORC). Khan et al. [20] examined numerically a PD cavity receiver with three different nanofluids, and the dish system was coupled with sCO<sub>2</sub> Brayton cycle to generate electricity. Abid et al. [21] performed an analysis of different sCO<sub>2</sub> recompression Brayton cycles. The heat source was a parabolic dish solar collector using pressurized water. Abid et al. [22] performed another study using different nanofluids and molten salts in parabolic trough and parabolic dish collectors to power a steam cycle.

The other HTFs utilized in the solar collector are the gases (air, helium, nitrogen, and CO<sub>2</sub>) and argon [23]. Super-critical carbon dioxide has attracted a lot of attention due to its extraordinary thermophysical properties. Its critical point is quite low (305 K and 7.8 MPa) that assists properties to enhance in the region adjacent to the triple point. Numerous studies proposed and recommended sCO<sub>2</sub> as a heat

transfer medium for higher temperature solar thermal applications [24–27].

Furthermore, the use of nanofluids in the solar collector enhances the rate of heat transfer that also raises the convective heat transfer coefficient, useful heat gain, and thermal efficiency of the solar collector. Mebarek-Oudina [28] numerically investigated laminar stationary natural convection heat transfer of different nanofluids contained in a cylindrical annulus using a discrete heat source. The objective was to investigate the effect of volume fraction, Rayleigh number, and base fluid type on the heat transfer rate. It was concluded that Raileigh number and volume fraction of nanoparticles has an influence on the thermal efficiency and growth rate of the heat transfer. Mebarek-Oudina [29] conducted a numerical investigation of natural convection heat transfer stability in vertical annulus using different heat source lengths. It was observed that heat transfer rates for smaller heater length are higher; however, heat transfer rate decreases by increasing the heater length. Kherbeet et al. [30] reported a numerical study of nanofluid flow and heat transfer of laminar convection flow adjacent to a horizontal and three-dimensional microscale forward facing step. It showed that the forward facing step increased the heat transfer, while Nusselt number also enhanced with rise in step height. Abbassi et al. [31] carried out a parametric investigation of a nanofluid-filled incinerator with a rectangular hot block on the bottom to evaluate the influence of different parameters (nanoparticle volume fraction, Rayleigh number, external magnetic intensity, etc.). It was concluded that increasing the width and height of the heater also enhanced the entropy generation but it has been reduced by increasing the Hartmann number. Goodarazi et al. [32] performed a study on the non-Newtonian nanofluid flow of carboxymethyl cellulose-aluminum oxide in a microtube. The aim was to explore the presence of nanoparticles and phenomenon of slip and temperature jump. Olia et al. [33] stated the modern developments on the applications of nanofluids for heat transfer fluid in parabolic trough solar collectors. It was concluded that nanofluids not only enhance the exergy efficiency, energy efficiency, and convective heat transfer coefficient but also mitigate the entropy generation of the system.

Gheynani et al. [34] examined the influence of nanoparticle concentration and diameter on the different heat transfer properties of non-Newtonian carboxymethyl cellulose/CuO fluid in a microtube using numerical simulation with the finite volume method. Taner [35] presented a bulgur drying plant based on the bulgur mass, temperature, and moisture for optimum production. Uncertainty analysis was carried out for data accuracy. The drying process energy and exergy efficiencies were found to be 24.95% and 44.05%, respectively. Taner [36] carried out an experimental optimization of a PEM fuel cell to enhance the efficiency and development of the simulations and modeling of PEM fuel cell. The first and second law efficiencies were almost 47.6% and 50.4%, respectively.

Topal et al. [37] performed a thermodynamic analysis of a trigeneration system that converted a single-fuel source into power, heating, and cooling and concentrated on the

simulation of such systems to a direct cocombustion of poultry wastes. It was found that cocombustion of poultry waste was the best environment-friendly remedy to put away wastes. Topal et al. [38] conducted a thermodynamic analysis of a can circulating fluidized bed power plant cofired with olive pits and to check the effect on exergy destruction and carbon dioxide emissions. Total exergy destruction of the plant was found to be 295 MW with 31.26% exergy efficiency. Taner and Sivrioglu [39] developed a general model for techno-economic and cost analysis of a turbine power plant. Simple payback period and unit cost for turbine power plant were calculated as 4.32 years and 3.142 \$/kW, respectively.

It is presented that there are many studies about the performance investigation of parabolic dish solar collector but there is lack of studies where both liquid and gas phase substances are evaluated simultaneously for their first and second law analyses. The aim of the present research is to examine in detail the energy and exergy efficiencies of PDSC using therminol VP1, pressurized water, and sCO<sub>2</sub> as heat transfer fluids. The thermal energy produced by the collector is further utilized to power a regenerative steam cycle for the purpose of electricity generation and rate of process heat. Therminol VP1 is a eutectic mixture of diphenyl oxide (DPO) and biphenyl. It can be used as a liquid heat transfer fluid or as a boiling-condensing heat transfer medium up to its maximum temperature. Various inlet temperature levels and mass flow rates are investigated to evaluate the work output, process heat rate, integrated efficiencies, and collector efficiencies of the solar integrated cogeneration plant. Different combinations of temperature and flow rate are tested for each heat transfer fluid, and at the end, a unique method of solar efficiency map is presented to depict the efficiencies of the solar receiver. The map shows the optimal conditions for the three HTFs exergetically and thermally with different operating temperature levels.

**1.1. System Description.** The proposed parabolic solar dish-integrated Rankine cycle producing electricity and rate of process heat is presented in Figure 1. Solar radiations from the sun and incidences on the aperture are reflected to the cavity receiver. The HTFs circulating inside the receiver takes the collected heat from the receiver. The high-temperature fluid at about 650 K moves to the boiler of steam cycle (point 9). The heated fluid transfers its heat to the water entering the boiler (point 5), circulating to the collector at relatively low temperature (point 10). Steam at higher pressure and higher temperature expands after passing through the turbine of a cogeneration plant (point 6). A small fraction (1/4<sup>th</sup>) of steam is extracted from the turbine (point 7) for process heating, while the remaining enters into the turbine to be expanded in the turbine (state point 8). The state of the liquid at the exit of the condenser is saturated, is pressurized using pump 1, and enters into the feed water heater (FWH) at higher pressure. A fraction of the steam after process heater (point 3) merges with the pressurized water in the feed water heater (FWH) and the mixture is pumped again towards the boiler for further process.

## 2. Methodology and Thermodynamic Analysis

The present section of the work is related to the mathematical equations, used for the thermodynamic modeling of PD solar receiver and regenerative Rankine cycle. Table 1 shows the input design parameters for the above said systems. A validated numerical mathematical model is developed with the help of the engineering equation solver (EES) [40]. The parabolic dish system presented in the present research is taken from Abid et al. [41], whereas Rankine cycle is adopted from [42]. The complete detail of both the systems can be found in the respective references.

**2.1. First and Second Law Analyses of Solar Parabolic Dish Collector.** The performance of the solar collector has an important role, and it is closely associated with the useful heat gain by the collector. The useful energy can be calculated using the following two equations:

$$\dot{Q}_u = \dot{m}C_p(T_{\text{out}} - T_{\text{in}}), \quad (1)$$

$$\dot{Q}_u = hA_{ri}(T_r - T_{fm}). \quad (2)$$

Amount of the solar energy available to the collector can be determined by

$$\dot{Q}_{\text{sun}} = G_b A_a. \quad (3)$$

The heat transfer coefficient ( $h$ ) between the working fluid in the solar collector and the receiver tube in equation (2) can be calculated using Nusselt number:

$$N_u = \frac{h.D_h}{k}. \quad (4)$$

Reynolds number is given by.

$$R_e = \frac{4\dot{m}}{\mu\pi D_{ri}}. \quad (5)$$

Gnielinski's correlation [43] for turbulent flow ( $3000 \leq R_e \leq 5 \times 10^6$  and  $0.5 \leq P_r \leq 2000$ ) is

$$N_U = \frac{(R_e - 1000)P_r(f_r/8)}{1 + 12.8 \left( \sqrt{(f_r/8)} \right) (P_r^{0.68} - 1)}. \quad (6)$$

The Prandtl number [44] and friction factor are evaluated as

$$P_r = \frac{\mu C_p}{k}, \quad (7)$$

$$f_r = (0.790 \ln - 1.64)^{-2}.$$

The energy efficiency of the dish collector is given by

$$\eta_{\text{en,PDSC}} = \frac{\dot{Q}_u}{\dot{Q}_{\text{sun}}}. \quad (8)$$

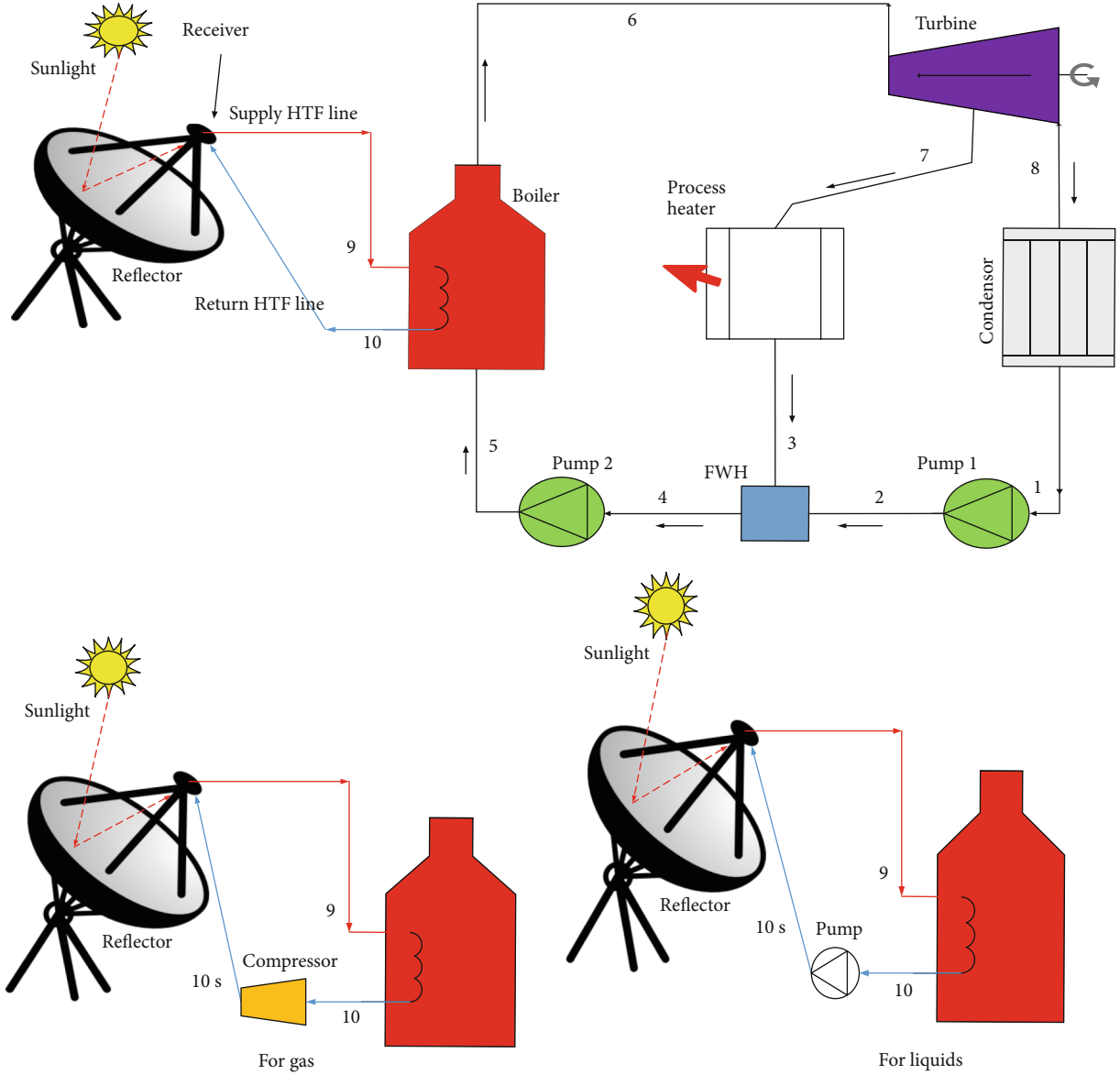


FIGURE 1: Schematic diagram of the proposed parabolic dish solar integrated cogeneration plant.

Another crucial parameter that is required to be determined is the output exergy of the solar receiver that is presented in equation (9). Exergy is the maximum possible work available from any process [45]. Equation (9) considers different parameters such as useful heat available, pressure losses, mass flow rate, and temperature [46].

$$\dot{E}_{x,u} = \dot{Q}_u - \dot{m}C_p T_{amb} \ln \left[ \frac{T_{out}}{T_{in}} \right] - \dot{m}T_{amb} \frac{\Delta P}{\rho_{fm} T_{fm}}. \quad (9)$$

The Petela model is the most established model to calculate the rate of solar exergy.

$$E_{x,sun} = G_b A_a \eta_{pet}, \quad (10)$$

$$\eta_{pet} = \left[ 1 - \frac{4T_0}{3T_{sun}} + \frac{1}{3} \left( \frac{T_0}{T_{sun}} \right)^4 \right].$$

Finally, exergy efficiency is found using exergy ratio between useful exergy and exergy of the sun.

$$\eta_{Ex,PDSC} = \frac{\dot{E}_{x,u}}{E_{x,sun}}. \quad (11)$$

The receiver's exergy destruction can be found using the below relation.

TABLE 1: Investigated system characteristics [41, 42].

$\eta_o$	85%
$\varepsilon_r$	90%
$\dot{m}$ (in solar collector)	0.02 kg/sec
$G_b$	1000 W/m <sup>2</sup>
$T_{in}$	350 K
$T_r$	540 K
$V_{air}$	1 m/sec
$T_a = T_0$	300 K
Outer and inner diameters of receiver tube	0.15 m & 0.015 m
Radius of dish, R	1.33 m
L	15 m
$T_s$	5700 K
$A_{ap}$	5.56 m <sup>2</sup>
$C_{rat}$	337
Insulation thickness	0.02 m
Steam mass flow rate through Rankine cycle	1 kg/sec
$\eta_{tur} = \eta_{pump}$	0.8
$T_{TIT}$ & $P_{TIT}$	773 K & 4000 kPa
Temperature and pressure of sCO <sub>2</sub> in collector	314-673 K & 10,000 kPa

$$\dot{\psi}_{x,des,\Delta_p} = T_a \frac{\dot{m} \Delta_p}{p} \frac{\ln(T_{out}/T_{in})}{T_{out} - T_{in}} \quad (12)$$

The heat gain of solar system is determined by the famous Hottel-Whillier equation [47].

$$\dot{Q}_u = F_r A_r \left[ \left( S - \frac{A_r}{A_a} \right) U_L (T_{in} - T_a) \right], \quad (13)$$

whereas heat removal factor and collector efficiency factor are summarized as

$$F_R = \frac{\dot{m} C_p}{A_r U_L} \left[ 1 - \exp \left( \frac{-A_r U_L F_1}{\dot{m} C_p} \right) \right], \quad (14)$$

$$F_1 = \frac{U_0}{U_L}.$$

**2.2. Energetic and Exergetic Analyses of Rankine Cycle.** Enthalpy is one of the most important parameters for steam cycle analysis. It is necessary to first calculate the enthalpy at each state of the system to calculate the rest of the output parameters. The efficiency of turbines is given as

$$\eta_{tur} = \frac{h_6 - h_7}{h_6 - h_{s,7}}, \quad (15)$$

$$\eta_{tur} = \frac{h_6 - h_8}{h_6 - h_{s,8}}.$$

TABLE 2: Comparison table for three HTFs at three inlet temperature levels.

$T_a = 300$ K			
$T_{in} = 350$ K	sCO <sub>2</sub>	Water	Therminol VP1
$\dot{m}_r = 0.02$ kg/sec			
$\dot{Q}_u$ (kW)	3898	4091	4013
$W_{net}$ (kW)	1104	1159	1137
$\dot{Q}_{pr,heat}$ (kW)	719.2	754.8	740.4
$T_a = 300$ K			
$T_{in} = 550$ K	sCO <sub>2</sub>	Water	Therminol VP1
$\dot{m}_r = 0.02$ kg/sec			
$\dot{Q}_u$ (kW)	3510	3599	3610
$W_{net}$ (kW)	994.3	1020	1023
$\dot{Q}_{pr,heat}$ (kW)	647.6	664	666.1
$T_a = 300$ K			
$T_{in} = 750$ K	sCO <sub>2</sub>	Water	Therminol VP1
$\dot{m}_r = 0.02$ kg/sec			
$\dot{Q}_u$ (kW)	3101	3170	3186
$W_{net}$ (kW)	878.5	898	902.5
$\dot{Q}_{pr,heat}$ (kW)	572.1	585	587.8

Work consumed by the pumps, to increase and circulate the pressure of working fluid, is given as

$$W_{p1} = v_1 \frac{[P_2 - P_1]}{\eta_{pump}}, \quad (16)$$

$$W_{p2} = v_4 \frac{[5 - P_4]}{\eta_{pump}}.$$

Work done by the turbine is given as

$$W_{Tur,out} = \dot{m}_6 (h_6 - h_7) + \dot{m}_8 (h_7 - h_8). \quad (17)$$

Heat input rate to the boiler and heat rejected by the condenser can be determined as [41]

$$Q_{in} = \dot{m}_5 \cdot (h_6 - h_5), \quad (18)$$

$$Q_{out} = \dot{m}_8 \cdot (h_8 - h_1).$$

The thermal energy for the process heater can be evaluated as

$$Q_{proc,heat} = \dot{m}_7 \cdot (h_7 - h_3). \quad (19)$$

The net power output of the cycle can be computed as

$$W_{net,cycle} = W_{Tur,out} - [W_{p1} + W_{p2}]. \quad (20)$$

The thermal or energy efficiency of the steam cycle is

TABLE 3: Thermodynamic properties of regenerative Rankine cycle.

State points	Enthalpy, $h$ (kJ/kg)	Pressure, $P$ (kPa)	Temperature, $T$ (K)	Entropy, $s$ (kJ/kg)	Mass flow rate (kg/sec)	Exergy, $Ex$ (kJ)
1	191.8	10	319	0.649	0.75	1.73
2	193.5	1200	319.1	0.650	0.75	2.65
3	798.3	1200	461.1	2.216	0.25	34.7
4	344.7	1200	355.2	1.1	1	20.09
5	348.8	4000	355.7	1.10	1	23.17
6	3446	4000	773	7.09	1	1323
7	3080	1200	588.8	7.09	0.25	239.5
8	2247	10	319	7.09	0.75	93.33

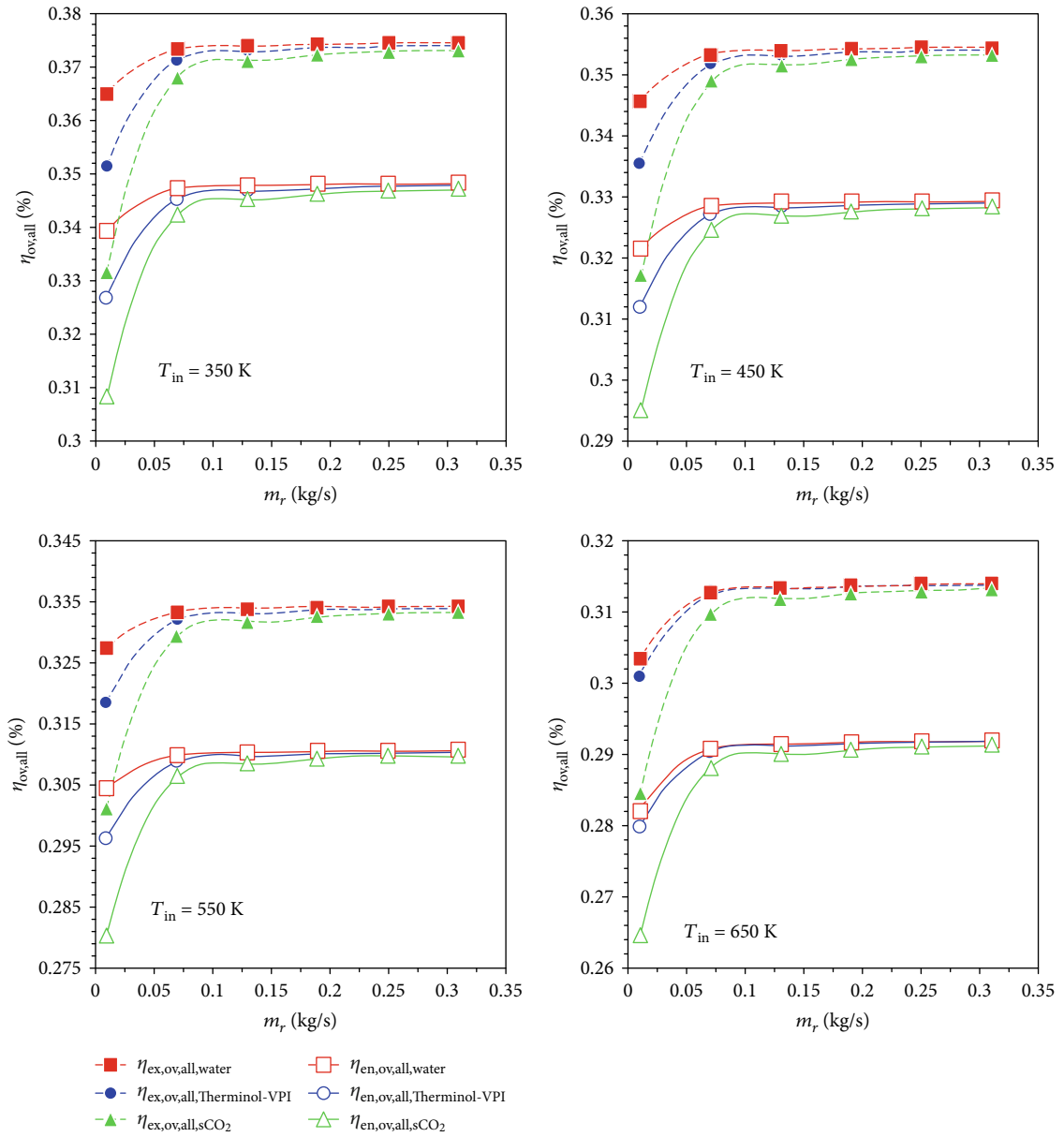


FIGURE 2: Effect of the mass flow rate on system-integrated efficiencies for various inlet temperature levels.

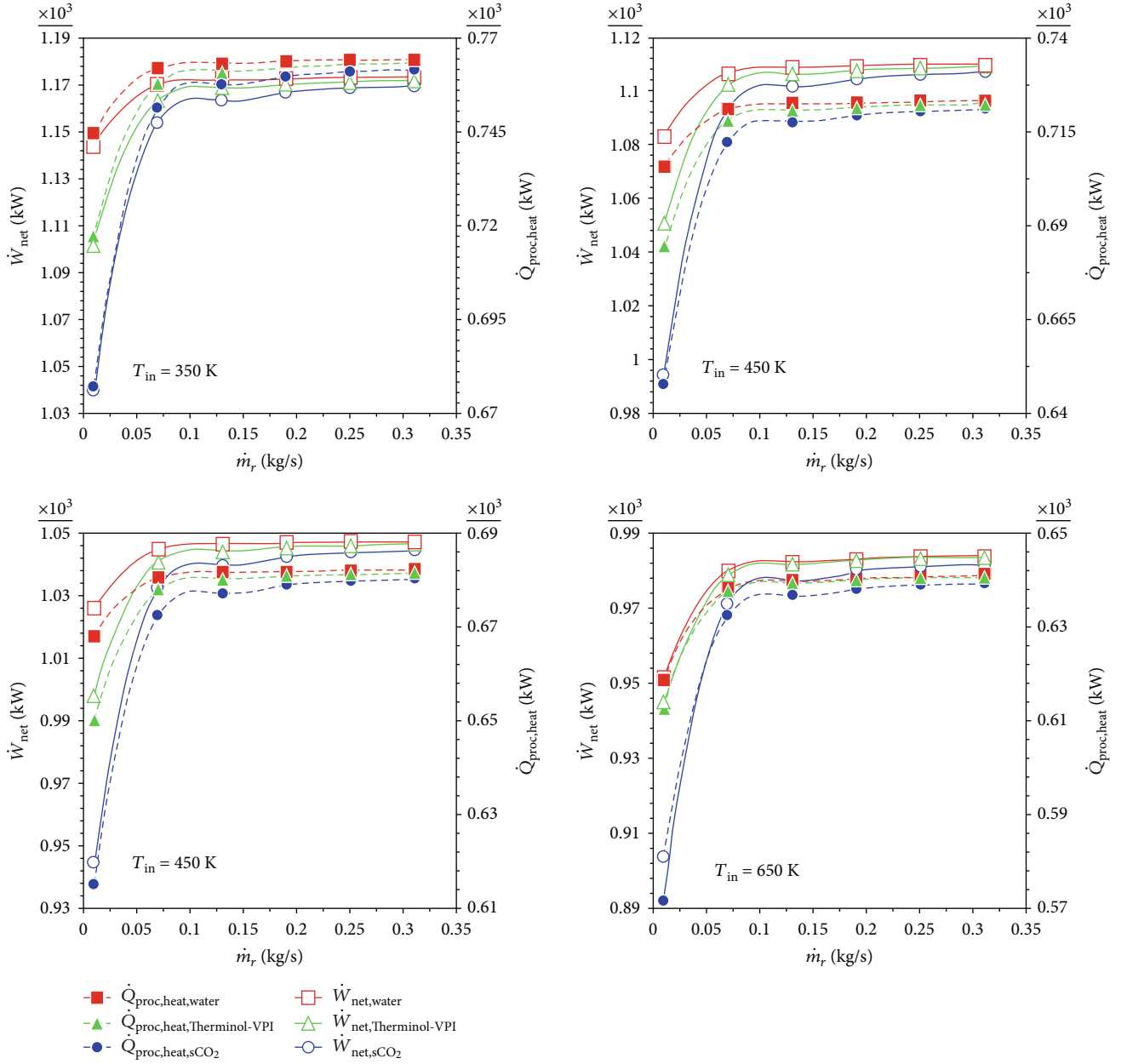


FIGURE 3: Effect of mass flow rate on net work and process heating for various inlet temperature levels.

determined as

$$\eta_{th} = \frac{W_{net,cycle} + Q_{proc,heat}}{Q_{in}} \quad (21)$$

Exergy values at all the points of the examined system are required to be determined in order to calculate the exergy destruction rate. Equation (22) gives the relation for exergy at relevant points.

$$\dot{E}_x = \dot{m}(h - h_0) - T_0(s - s_0). \quad (22)$$

The exergy supplied to the boiler and condenser is mea-

sured as

$$\begin{aligned} \dot{E}x_{th,b} &= \left[1 - \frac{T_0}{T_b}\right] \cdot \dot{Q}_b, \\ \dot{E}x_{th,c} &= \left[1 - \frac{T_0}{T_c}\right] \cdot \dot{Q}_c. \end{aligned} \quad (23)$$

Finally, exergy efficiency of the steam cycle and system-integrated efficiencies are given as

$$\eta_x = \frac{W_{net,cycle} + Q_{proc,heat}}{\dot{E}x_{th,b}}, \quad (24)$$

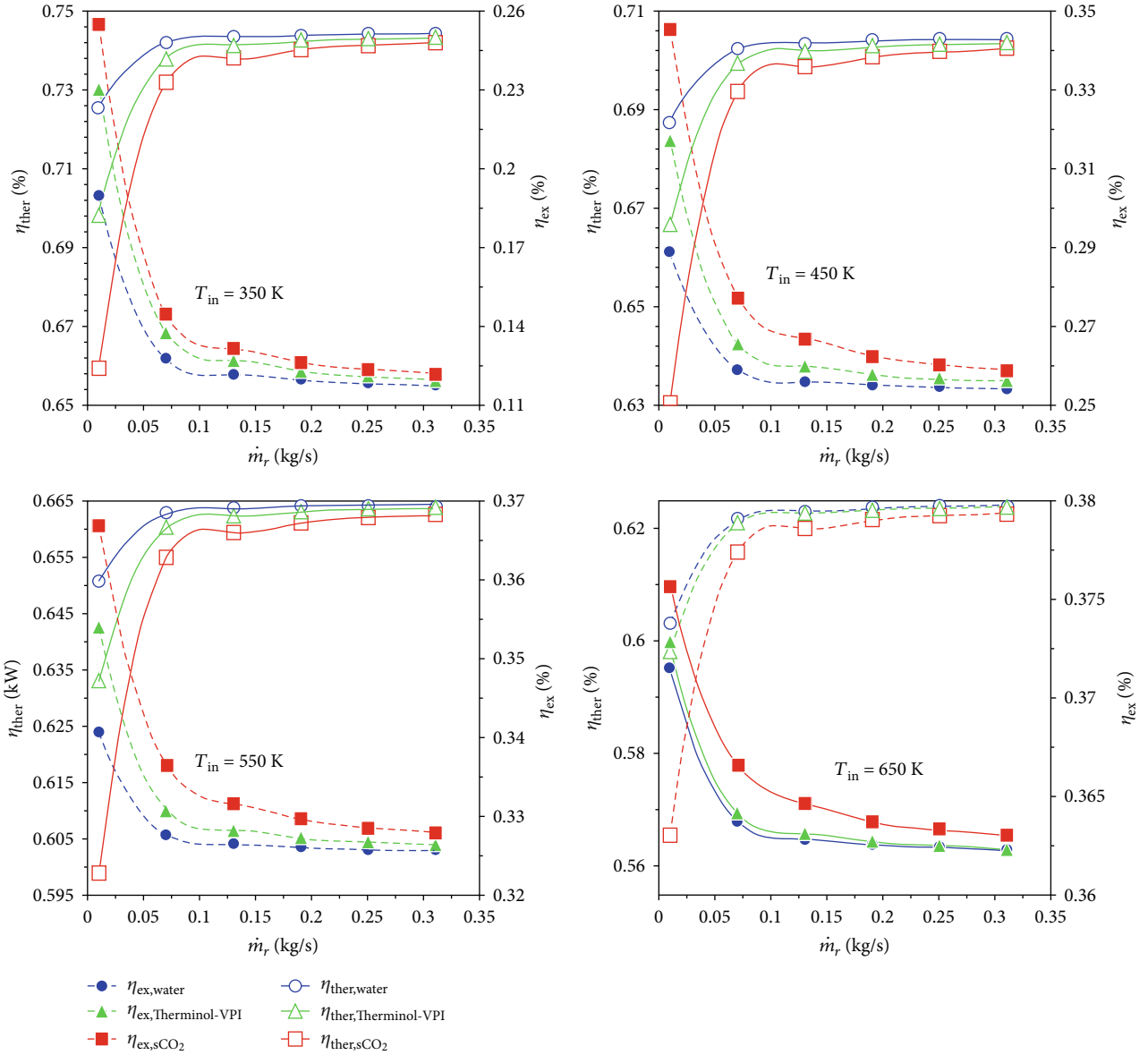


FIGURE 4: Effect of mass flow rate on the thermal and exergy efficiencies for various inlet temperature levels.

$$\eta_{en,ovall} = \frac{W_{net,cycle} + Q_{proc,heat}}{\dot{Q}_{solar}}, \quad (25)$$

$$\eta_{ex,ovall} = \frac{W_{net,cycle} + Q_{proc,heat}}{\dot{E}x_{solar}}. \quad (26)$$

### 3. Results and Discussion

This study concentrates on the integration of the parabolic dish solar collector utilizing three different HTFs, namely,  $sCO_2$ , therminol VPI, and pressurized water with regenerative Rankine cycle, generating electricity and process heat. The present section discusses the findings of the investigated system in details. The change in mass flow rate at different inlet temperature levels of three heat transfer fluids in the solar collector is examined. The performance parameters considered in the study are overall energetic and exergetic

efficiencies, power output and rate of process heat, receiver thermal and exergy efficiencies, and convective heat transfer coefficient. The steam Rankine cycle produces 875 kW of electricity and 570 kW heat for processing, and its thermal and exergy efficiencies are found to be 46.7% and 76.3%, respectively. Table 2 below shows the useful heat gain by the solar collector, net power produced, and process heat rate for the examined HTFs at three different inlet temperature levels. It is evident from the table that for lower inlet temperature, water is a better working fluid; however its effectiveness becomes less at higher temperatures. The performance of therminol VPI gets better at elevated temperatures of above 550 K, while  $sCO_2$  also performs well at upper temperature levels. Thermodynamic properties of regenerative Rankine cycle are presented in Table 3.

Figure 2 illustrates the variation of system-integrated efficiencies for a range of inlet temperature from 350 K to 650 K.



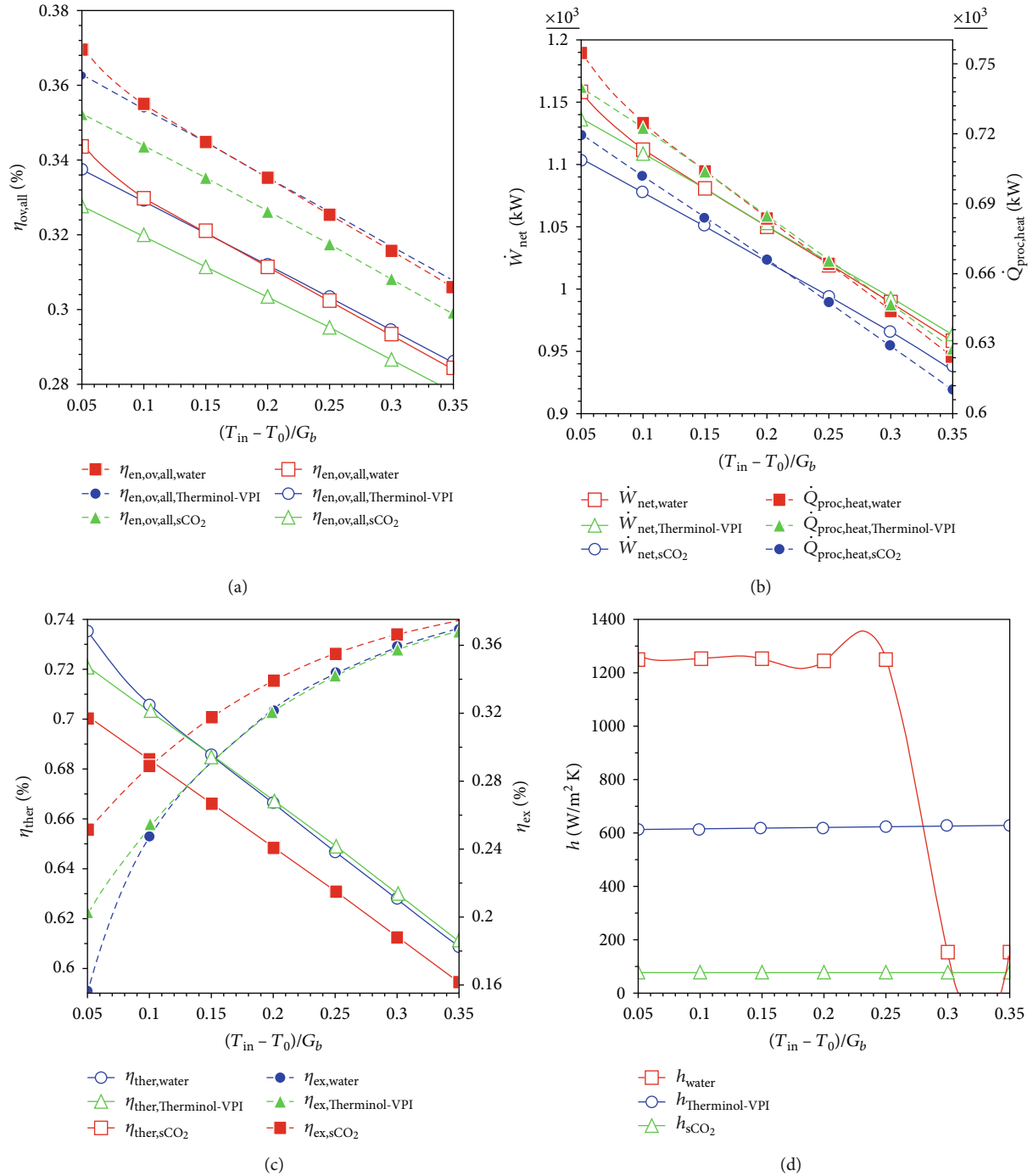


FIGURE 5: Effect on Inlet temperature on (a) integrated efficiencies, (b) net work output and process heating, (c) thermal and exergy efficiencies, and (d) heat transfer coefficient.

These graphs can be explained in many ways. It can be seen that higher flow rate and lower temperature gives maximum overall energy and exergy efficiencies for the investigated HTFs. However, for a mass flow rate of above 0.15 kg/sec, the variation in the properties becomes stagnant, meaning that there is no reason for employing higher mass flow rate from a thermal point of view. According to equation (25), overall energy efficiency of the integrated system is the ratio of work output from turbine and process heat rate of the pro-

cess heater to the energy of the solar. Furthermore, higher value of the numerator depends on higher amount of useful heat by the solar collector according to equation (1).

Furthermore, for all the inlet temperature levels, integrated efficiencies of pressurized water are the highest as compared to the other investigated fluids. The maximum difference in efficiency values of HTFs is seen at nearly 0.01 kg/sec, but after that, this difference reduces continuously. At a mass flow rate of 0.3 kg/sec, the efficiency of all

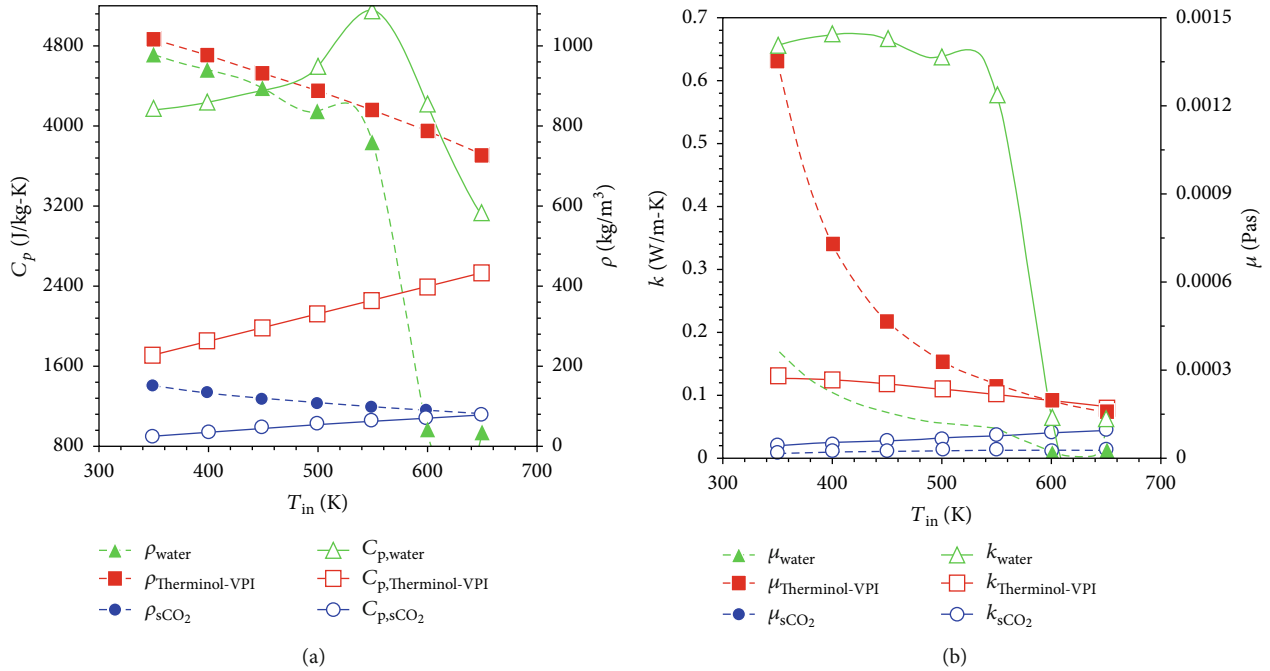


FIGURE 6: Comparison of properties (a) density and specific heat capacity and (b) thermal conductivity and viscosity.

the investigated fluids converges on the same point. At inlet temperature of 650 K, efficiency of therminol VP1 approaches very near to water values because the performance of water becomes less efficient after 600 K [24]. Pressurized water is witnessed to have 3.85% and 10% higher efficiency than the therminol VP1- and  $sCO_2$ -based HTFs, respectively, at a mass flow rate of 0.01 kg/sec. However, these values are reduced to 0.11% and 0.31% at higher mass flow rate of 0.3 kg/sec.

Figure 3 is related to the variation of mass flow rate and its influence on net power produced and rate of process heat at four different inlet temperature levels. Both the performance parameters increase sharply between 0.01 and 0.15 kg/sec and after that remain constant until 0.3 kg/sec. It is evident from Figure 3 that higher values are obtained at lower inlet temperature, and pressurized water is observed to have the highest rate of process heat and work output than the other two investigated HTFs. Net power output utilizing pressurized water in the collector loop is increased to 2.44% for a range of flow rate from 0.01 and 0.15 kg/sec; however, after 0.15 to 0.3 kg/sec, the increment is found to be as low as 0.17%. Therminol VP1 and  $sCO_2$  has 6% and 11.9% increase for 0.01 to 0.15 kg/sec but very less increment in work output (0.17% and 0.51%, respectively). Further rise in mass flow rate clearly indicates that after a certain point, increase in mass flow rate has no importance for thermal enhancement. The highest variation is seen for  $sCO_2$  values at all inlet temperatures due to its behavior near critical region [20]. Highest amount of work produced and rate of process heat is obtained for pressurized water at 350 K that is 1173 kW and 764 kW, respectively. For higher inlet temperature of 650 K, almost 19% reduction is found for both performance parameters.

Figure 4 depicts the influence of the mass flow rate on the thermal and exergetic efficiencies of the parabolic dish receiver at four inlet temperature levels. Thermal efficiency of all investigated fluids has the same trend as discussed above for other performance parameters but exergy efficiency behaves in an opposite way with the rise in mass flow rate. PD collector with water as a HTF has the highest thermal efficiency (74.43%) at 350 K and at a mass flow rate of 0.3 kg/sec, while lowest value has been found for  $sCO_2$  (74.2%). From the exergetic point of view,  $sCO_2$  has a dominant feature as compared to the other HTFs and highest exergy efficiency (37.56%) is noticed at higher temperature (650 K) and lower flow rate (0.01 kg/sec). The highest exergy efficiency value of  $sCO_2$  is due to its lower specific heat capacity as compared to therminol VP1 and pressurized water [23]. Exergy efficiency is the ratio of collector useful exergy to the exergy available from solar [22] and higher inlet temperature of fluid in the receiver will deliver maximum exergy but solar exergy is independent of the inlet temperature and remains the same for all the values of the temperature. The collector exergy depends on useful heat gain from collector, mass flow rate, and temperatures of fluid as followed by equation (9).

Figures 5(a)–5(d) represent the simulation results of integrated system efficiencies, work output, and process heat rate and collect performance as well as the heat transfer coefficient with respect to the inlet temperature. The operational parameter  $(T_{in} - T_0)/G_b$  is a parameter expressing the collector efficiency. It reflects the inlet temperature of HTFs as direct normal irradiation, and ambient temperature remained constant during the simulation. The obtained results are considered at ambient temperature of 300 K, DNI of 1000 W/m<sup>2</sup>, and flow rate of 0.02 kg/sec. The inlet temperature increases between 350 K and 650 K with a step

TABLE 4: Optimum operating conditions for the three examined HTFs at different inlet temperatures.

$T_{in}$ (K)	$\dot{m}_{in,op}$ (kg/sec)	$\eta_{th}$			$\eta_{ex}$		
		sCO <sub>2</sub>	Water	Therminol VP1	sCO <sub>2</sub>	Water	Therminol VP1
350	0.07	0.7319	0.7421	0.7381	0.1683	0.1275	0.1447
450	0.07	0.6936	0.7023	0.6993	0.2773	0.2588	0.2657
550	0.20	0.661	0.6642	0.6632	0.3296	0.326	0.3272
650	0.30	0.6228	0.6241	0.6239	0.363	0.3622	0.3623
750	0.30	0.5829	0.5837	0.5839	0.3776	0.3775	0.3775
850	0.30	0.543	0.5438	0.5439	0.33	0.3265	0.3276

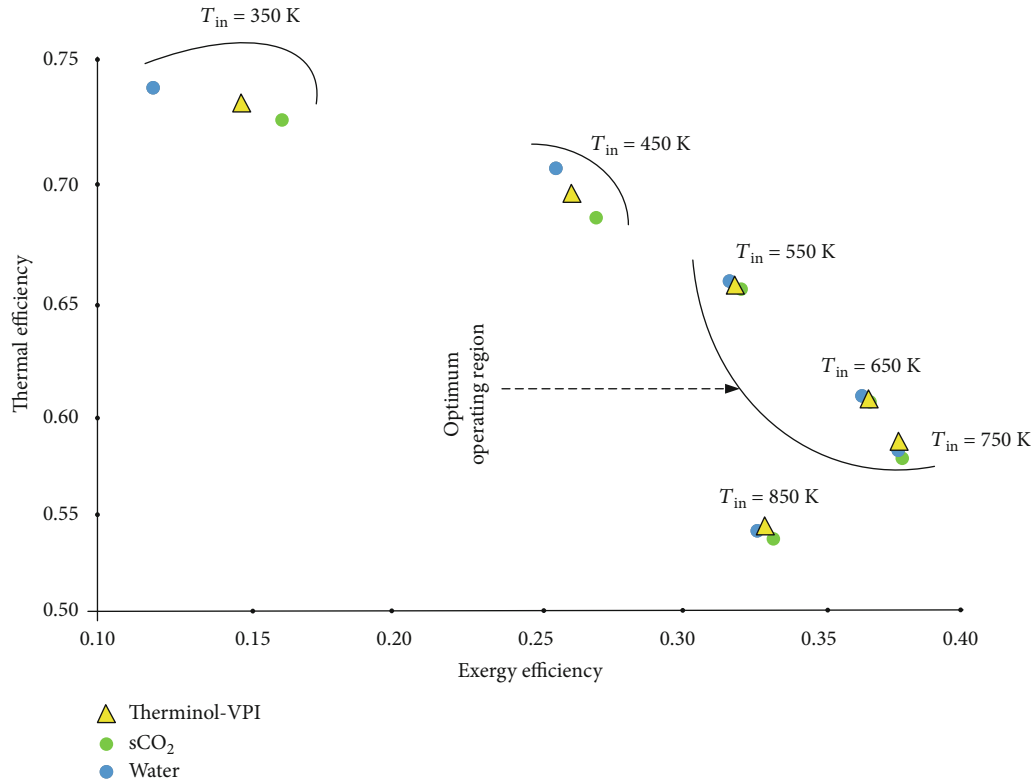


FIGURE 7: Efficiency map of PDSC for the three investigated fluids at various inlet temperature levels.

50 K. Higher values of inlet temperature offers greater temperature of the receiver surface that results in maximum heat losses from the receiver surface. Higher heat losses decreases the useful heat production from the collector which eventually results in lowering the net power produced and process heat rate of the system.

In Figure 5(a), overall energy and exergy efficiencies of the integrated system employing water reduce from 34.4% to 28.5% and 37% to 30.6%, respectively, and it shows reduction of almost 20.8%. The same trend is noticed for the therminol VP1- and sCO<sub>2</sub>-based integrated systems with decrease of nearly 17.93% and 17.87%, accordingly. Pressurized water was found to be 1.95% and 4.95% efficient than the systems operated with therminol VP1 and sCO<sub>2</sub>, respectively, at 350 K. However, after 500 K, the performance of the system using water as HTF reduces, and at 650 K, therminol VP1 was found to be 0.52% better than water. Similarly,

Figure 5(b) has a very similar trend as described above; therminol VP1 has a dominant role at elevated temperatures. Collector thermal efficiency presented in Figure 5(c) has a very similar behavior to the work output and integrated efficiencies, i.e., higher thermal efficiency is found at lower temperature of 350 K. However, for exergy efficiency, sCO<sub>2</sub>-based collector has the highest value among the other compared HTFs. Maximum value is recorded for sCO<sub>2</sub>, therminol VP1, and water with 37.37%, 36.86%, and 36.98%, respectively, at 650 K. Figure 5(d) shows the graphical representation of the convective heat transfer coefficient of the absorber and investigated HTFs. It is clear that sCO<sub>2</sub> has the lowest value of  $h$  as compared to the other HTFs. The heat transfer coefficient ( $h$ ) of therminol VP1 is more stable at all the temperature levels, while for water,  $h$  is constant at lower temperatures and after 500 K, and it drops dramatically due to evaporation.

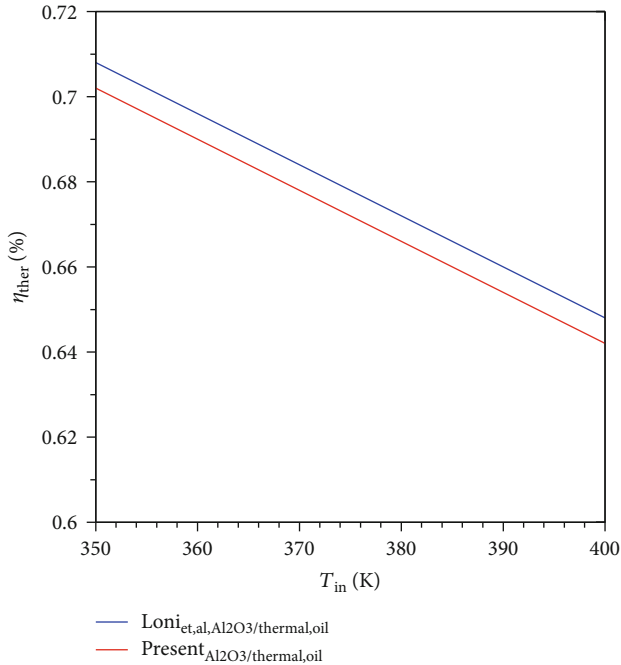


FIGURE 8: Validation of solar dish collector model with Loni et al. [48].

Figure 6(a) is the portrayal of density and heat capacity of three investigated fluids. The  $C_p$  values of pressurized water have an upward trend at low temperatures; however, a sudden decrease is observed after 550 K, while  $sCO_2$  has shown an increment of nearly 23.3%. The synthetic oil is found to have better thermophysical properties, as  $C_p$  of the therminol increases by 48.5 with a rise in temperature. A decrease in the density of all HTFs is found with the rise in temperature. Maximum value of density can be seen for oil at lower temperature, and a constant fall is found for  $sCO_2$  as well, while water depicts a dramatic change after 550 K [41]. Thermal conductivity values in Figure 6(b) shows the similar tendency to that of viscosity; maximum  $k$  value can be seen at 400 K for water and a reduction can be observed afterwards. Thermal conductivity of oil reduces to 61.5%, while a small increase for  $sCO_2$  is noticed.

The following section provides the optimum operating conditions for the investigated heat transfer fluids in solar dish collector at various inlet temperature levels. The combinations of mass flow rate and inlet temperature of the working fluid in the receiver that lead to higher thermal and exergy efficiency will be assumed the optimum conditions. Table 4 and Figure 7 consist of the outcomes for optimal values against all levels of inlet temperatures. For low-temperature levels of up to 450 K, the optimum flow rate is 0.07 kg/sec and corresponding efficiency values are tabulated in front of them. At 550 K, the optimum value of the mass flow rate can be seen to be 0.20 kg/sec, while higher inlet temperatures have optimum features at 0.30 kg/sec. The highest value of the exergetic efficiency for all the three investigated fluids is obtained at 750 K with flow rate of 0.30 kg/sec; however, a higher value of thermal efficiency is witnessed at 350 K

and 0.07 kg/sec. This table also proves that the highest exergy performance does not associate with the higher thermal efficiency, and hence, the optimal operating scenario can be selected by taking both energy and exergy into consideration. The efficiency map of the collector is very useful and is an innovative tool to evaluate the collector performance under different criteria. Furthermore, validation of the parabolic dish receiver has been conducted by comparing the thermal efficiency of the collector using  $Al_2O_3$ /thermal oil as a HTF with the model presented by Loni et al. [48] in Figure 8. The proposed model shows a discrepancy of 0.85% in efficiency in comparison to the reference model when evaluated against inlet temperature.

#### 4. Conclusions

Thermodynamic performance investigation of PD solar-assisted cogeneration plant is presented in this study. Three working fluids/HTFs, namely,  $sCO_2$ , pressurized water, and therminol VP1, are used to collect the heat produced by the solar collector. The collected heat is further used to drive the regenerative steam Rankine cycle producing power and process heat simultaneously. Firstly, PDSC is thermodynamically modeled by considering three HTFs ( $sCO_2$ , pressurized water, and therminol VP1) and those modeling results are further utilized to evaluate the performance of integrated system. Different combinations of flow rates and inlet temperatures have been tested and an optimal scenario is presented that leads to maximum energy and exergy efficiencies of the solar collector. The major outcomes are presented as follows:

- (i) Higher flow rate and lower temperature offer maximum overall energy and exergy efficiencies for the investigated HTFs. Pressurized water is observed to have an integrated efficiency of 10% and 3.85% higher than  $sCO_2$ - and therminol VP1-based HTFs, respectively, at a flow rate of 0.01 kg/sec. However, these values are reduced to 0.11% and 0.31% at a higher flow rate of 0.3 kg/sec
- (ii) Net power output of the proposed integrated system for water as a HTF in the collector loop is increased to 2.44% for flow rate from 0.01 to 0.15 kg/sec; however, after 0.15 to 0.3 kg/sec, this increment is as low as 0.17%. Therminol VP1 and  $sCO_2$  has 6% and 11.9% increase for flow rate between 0.01 and 0.15 kg/sec but very less increment in work output values (0.17% and 0.51%, respectively) for further rise in the mass flow rate. Highest amount of net power produced (1173 kW) and the rate of process heat (764 kW) are obtained for pressurized water at 350 K, respectively. For higher inlet temperature of 650 K, almost 19% reduction is found for both performance parameters
- (iii) The PD collector with water as a HTF has the highest thermal efficiency (74.43%) at 350 K and at a flow rate of 0.3 kg/sec, while lowest value has been found for  $sCO_2$  (74.2%). From the exergetic point of view, the  $sCO_2$  outperforms the other heat transfer fluids

- (iv) Pressurized water was found to be 1.95% and 4.95% more efficient than the systems operating with therminol VP1 and sCO<sub>2</sub>, working fluids at a temperature of 350 K. However, the performance of the system using water as HTF starts to decrease with rise in temperature, and at 650 K, therminol VP1 is observed to surpass water with 0.52% better efficiency
- (v) An innovative solar efficiency map is proposed with an aim to find out the optimal operating region with respect to collector energy and exergy efficiencies. The maximum exergy efficiency of 37.75% is observed at a temperature of 750 K and at a flow rate of 0.3 kg/sec

## Nomenclature

### Acronyms

CSP: Concentrated solar power  
 CFD: Computational fluid dynamics  
 FWH: Feed water heater  
 HTFs: Heat transfer fluids  
 PDC: Parabolic dish collector  
 sCO<sub>2</sub>: Supercritical carbon dioxide.

### Symbols

$A_a$ : Area of aperture (m<sup>2</sup>)  
 $A_{ri}$ : Area of receiver (m<sup>2</sup>)  
 $C_p$ : Specific heat capacity (J/kg-K)  
 $D_h$ : Hydraulic diameter (m)  
 $\dot{E}_{x,u}$ : Useful exergy  
 $f_r$ : Friction factor  
 $F_r$ : Heat removal factor  
 $F_1$ : Collector efficiency factor  
 $G_b$ : Solar radiation (W/m<sup>2</sup>)  
 $h$ : Enthalpy (kJ/kg)  
 $k$ : Thermal conductivity (W/m-K)  
 $\dot{m}$ : Mass flow rate (kg/sec)  
 $Pr$ : Prandtl number  
 $\dot{Q}_u$ : Useful heat (kW)  
 $\dot{Q}_b$ : Heat rate of boiler (kW)  
 $T_{fm}$ : Mean fluid temperature (K)  
 $U_L$ : Coefficient of heat loss (W/m<sup>2</sup> K).

### Greek Letters

$\eta_{\text{pump}}$ : Pump efficiency (%)  
 $\eta_{\text{tur}}$ : Turbine efficiency (%)  
 $\rho$ : Density (kg/m<sup>3</sup>)  
 $\eta_{\text{pet}}$ : Petela efficiency  
 $\eta_{\text{en}}$ : Energy efficiency (%)  
 $\psi$ : Rate of exergy destruction (kW).

## Data Availability

Data will be provided on request.

## Conflicts of Interest

The authors declare that they have no conflicts of interest.

## Acknowledgments

The authors wish to express their great appreciation for the financial support from the National International Cooperation Project, China (2016YFE0202000 and 2017YFE0107600), National Natural Science Foundation of China (51976196), and International Cooperation Project of Zhejiang Province (2019C04026).

## References

- [1] I. M. Yusri, R. Mamat, G. Najafi et al., "Alcohol based automotive fuels from first four alcohol family in compression and spark ignition engine: a review on engine performance and exhaust emissions," *Renewable and Sustainable Energy Reviews*, vol. 77, pp. 169–181, 2017.
- [2] A. R. Keeley and K. I. Matsumoto, "Investors' perspective on determinants of foreign direct investment in wind and solar energy in developing economies - Review and expert opinions," *Journal of Cleaner Production*, vol. 179, pp. 132–142, 2018.
- [3] S. Pavlovic, A. M. Daabo, E. Bellos, V. Stefanovic, S. Mahmoud, and R. K. Al-Dadah, "Experimental and numerical investigation on the optical and thermal performance of solar parabolic dish and corrugated spiral cavity receiver," *Journal of Cleaner Production*, vol. 150, pp. 75–92, 2017.
- [4] M. Abid, M. S. Khan, and T. A. H. Ratlamwala, "Comparative energy, exergy and exergo-economic analysis of solar driven supercritical carbon dioxide power and hydrogen generation cycle," *International Journal of Hydrogen Energy*, vol. 45, no. 9, pp. 5653–5667, 2020.
- [5] M. S. Khan, K. P. Amber, H. M. Ali, M. Abid, T. A. Ratlamwala, and S. Javed, "Performance analysis of solar assisted multigenerational system using therminol VP1 based nanofluids: a comparative study," *Thermal Science*, vol. 24, no. 2 Part A, pp. 865–878, 2020.
- [6] J. Coventry and C. Andraka, "Dish systems for CSP," *Solar Energy*, vol. 152, pp. 140–170, 2017.
- [7] A. M. Daabo, S. Mahmoud, and R. K. Al-Dadah, "The effect of receiver geometry on the optical performance of a small-scale solar cavity receiver for parabolic dish applications," *Energy*, vol. 114, pp. 513–525, 2016.
- [8] E. Przenzak, M. Szubel, and M. Filipowicz, "The numerical model of the high temperature receiver for concentrated solar radiation," *Energy Conversion and Management*, vol. 125, pp. 97–106, 2016.
- [9] R. D. Jilte, S. B. Kedare, and J. K. Nayak, "Investigation on convective heat losses from solar cavities under wind conditions," *Energy Procedia*, vol. 57, pp. 437–446, 2014.
- [10] N. D. Kaushika and K. S. Reddy, "Performance of a low cost solar paraboloidal dish steam generating system," *Energy Conversion and Management*, vol. 41, no. 7, pp. 713–726, 2000.
- [11] R. Loni, A. B. Kasaian, E. A. Asli-Ardeh, B. Ghobadian, and W. G. Le Roux, "Performance study of a solar-assisted organic Rankine cycle using a dish-mounted rectangular-cavity tubular solar receiver," *Applied Thermal Engineering*, vol. 108, pp. 1298–1309, 2016.

- [12] A. Mawire and S. H. Taole, "Experimental energy and exergy performance of a solar receiver for a domestic parabolic dish concentrator for teaching purposes," *Energy for Sustainable Development*, vol. 19, pp. 162–169, 2014.
- [13] I. L. Mohammed, "Design and development of a parabolic dish solar water heater," *International Journal of Engineering Research and Applications*, vol. 2, no. 1, pp. 822–830, 2012.
- [14] K. S. Reddy, S. K. Natarajan, and G. Veershetty, "Experimental performance investigation of modified cavity receiver with fuzzy focal solar dish concentrator," *Renewable Energy*, vol. 74, pp. 148–157, 2015.
- [15] V. Madadi, T. Tavakoli, and A. Rahimi, "First and second thermodynamic law analyses applied to a solar dish collector," *Journal of Non-Equilibrium Thermodynamics*, vol. 39, no. 4, pp. 183–197, 2014.
- [16] E. Bellos, C. Tzivanidis, and K. A. Antonopoulos, "A detailed working fluid investigation for solar parabolic trough collectors," *Applied Thermal Engineering*, vol. 114, pp. 374–386, 2017.
- [17] M. Abid, T. A. H. Ratlamwala, and U. Atikol, "Performance assessment of parabolic dish and parabolic trough solar thermal power plant using nanofluids and molten salts," *International Journal of Energy Research*, vol. 40, no. 4, pp. 550–563, 2016.
- [18] R. Loni, E. A. Asli-Ardeh, B. Ghobadian, E. Bellos, and W. G. Le Roux, "Numerical comparison of a solar dish concentrator with different cavity receivers and working fluids," *Journal of Cleaner Production*, vol. 198, pp. 1013–1030, 2018.
- [19] R. Loni, A. B. Kasaeian, E. A. Asli-Ardeh, and B. Ghobadian, "Optimizing the efficiency of a solar receiver with tubular cylindrical cavity for a solar-powered organic Rankine cycle," *Energy*, vol. 112, pp. 1259–1272, 2016.
- [20] M. S. Khan, M. Abid, H. M. Ali, K. P. Amber, M. A. Bashir, and S. Javed, "Comparative performance assessment of solar dish assisted s-CO<sub>2</sub> Brayton cycle using nanofluids," *Applied Thermal Engineering*, vol. 148, pp. 295–306, 2019.
- [21] M. Abid, M. S. Khan, and T. A. Ratlamwala, "Techno-environmental analysis of a parabolic dish assisted recompression with and without reheat s-CO<sub>2</sub> Brayton cycle," *International Journal of Exergy*, vol. 27, no. 4, pp. 527–552, 2018.
- [22] M. Abid, T. A. Ratlamwala, and U. Atikol, "Solar assisted multi-generation system using nanofluids: a comparative analysis," *International Journal of Hydrogen Energy*, vol. 42, no. 33, pp. 21429–21442, 2017.
- [23] E. Bellos, C. Tzivanidis, K. A. Antonopoulos, and I. Daniil, "The use of gas working fluids in parabolic trough collectors—an energetic and exergetic analysis," *Applied Thermal Engineering*, vol. 109, pp. 1–14, 2016.
- [24] E. C. Okonkwo, M. Abid, and T. A. Ratlamwala, "Numerical analysis of heat transfer enhancement in a parabolic trough collector based on geometry modifications and working fluid usage," *Journal of Solar Energy Engineering*, vol. 140, no. 5, article 051009, 2018.
- [25] M. Atif and F. A. Al-Sulaiman, "Energy and exergy analyses of solar tower power plant driven supercritical carbon dioxide recompression cycles for six different locations," *Renewable and Sustainable Energy Reviews*, vol. 68, pp. 153–167, 2017.
- [26] Y. Qiu, M. J. Li, Y. L. He, and W. Q. Tao, "Thermal performance analysis of a parabolic trough solar collector using supercritical CO<sub>2</sub> as heat transfer fluid under non-uniform solar flux," *Applied Thermal Engineering*, vol. 115, pp. 1255–1265, 2017.
- [27] R. Aguilar, L. Valenzuela, A. L. Avila-Marin, and P. L. Garcia-Ybarra, "Simplified heat transfer model for parabolic trough solar collectors using supercritical CO<sub>2</sub>," *Energy Conversion and Management*, vol. 196, pp. 807–820, 2019.
- [28] F. Mebarek-Oudina, "Convective heat transfer of Titania nanofluids of different base fluids in cylindrical annulus with discrete heat source," *Heat Transfer - Asian Research*, vol. 48, no. 1, pp. 135–147, 2019.
- [29] F. Mebarek-Oudina, "Numerical modeling of the hydrodynamic stability in vertical annulus with heat source of different lengths," *Engineering science and technology, an international journal*, vol. 20, no. 4, pp. 1324–1333, 2017.
- [30] A. S. Kherbeet, H. A. Mohammed, H. E. Ahmed et al., "Mixed convection nanofluid flow over microscale forward-facing step—effect of inclination and step heights," *International Communications in Heat and Mass Transfer*, vol. 78, pp. 145–154, 2016.
- [31] M. A. Abbassi, M. R. Safaei, R. Djebali, K. Guedri, B. Zeghamati, and A. A. Alrashed, "LBM simulation of free convection in a nanofluid filled incinerator containing a hot block," *International Journal of Mechanical Sciences*, vol. 144, pp. 172–185, 2018.
- [32] M. Goodarzi, S. Javid, A. Sajadifar et al., "Slip velocity and temperature jump of a non-Newtonian nanofluid, aqueous solution of carboxy-methyl cellulose/aluminum oxide nanoparticles, through a microtube," *International Journal of Numerical Methods for Heat and Fluid Flow*, vol. 29, no. 5, pp. 1606–1628, 2019.
- [33] H. Olia, M. Torabi, M. Bahiraei, M. H. Ahmadi, M. Goodarzi, and M. R. Safaei, "Application of nanofluids in thermal performance enhancement of parabolic trough solar collector: state-of-the-art," *Applied Sciences*, vol. 9, no. 3, p. 463, 2019.
- [34] A. R. Gheynani, O. A. Akbari, M. Zarringhalam et al., "Investigating the effect of nanoparticles diameter on turbulent flow and heat transfer properties of non-Newtonian carboxymethyl cellulose/CuO fluid in a microtube," *International Journal of Numerical Methods for Heat and Fluid Flow*, vol. 29, no. 5, pp. 1699–1723, 2019.
- [35] T. Taner, "Optimisation processes of energy efficiency for a drying plant: a case of study for Turkey," *Applied Thermal Engineering*, vol. 80, pp. 247–260, 2015.
- [36] T. Taner, "Energy and exergy analyze of PEM fuel cell: a case study of modeling and simulations," *Energy*, vol. 143, pp. 284–294, 2018.
- [37] H. Topal, T. Taner, Y. Altuncı, and E. Amirabedin, "Application of trigeneration with direct co-combustion of poultry waste and coal: a case study in the poultry industry from Turkey," *Thermal Science*, vol. 22, no. 6 Part B, pp. 3073–3082, 2018.
- [38] H. Topal, T. Taner, S. A. H. Naqvi, Y. Altunsoy, E. Amirabedin, and M. Ozkaymak, "Exergy analysis of a circulating fluidized bed power plant co-firing with olive pits: a case study of power plant in Turkey," *Energy*, vol. 140, pp. 40–46, 2017.
- [39] T. Taner and M. Sivrioglu, "A techno-economic & cost analysis of a turbine power plant: a case study for sugar plant," *Renewable and Sustainable Energy Reviews*, vol. 78, pp. 722–730, 2017.
- [40] S. A. Klein, *Engineering equation solver, v8.411*, F-Chart Software, Madison, Wisconsin, 2009.

- [41] M. Abid, M. S. Khan, T. A. H. Ratlamwala, and K. P. Amber, "Thermo-environmental investigation of solar parabolic dish-assisted multi-generation plant using different working fluids," *International Journal of Energy Research*, vol. 44, no. 15, pp. 12376–12394, 2020.
- [42] A. Cengel Younus and M. A. Boles, *Thermodynamics: An Engineering Approach*, McGraw-Hill, New York, NY, USA, 7th edition, 2017, in SI units.
- [43] V. Gnielinski, "New equations for heat and mass transfer in turbulent pipe and channel flow," *International Chemical Engineering*, vol. 16, no. 2, pp. 359–368, 1976.
- [44] T. L. Bergman, A. S. Lavine, F. P. Incropera, and D. P. Dewitt, *Fundamentals of Heat and Mass Transfer*, John Wiley & Sons, 2011.
- [45] I. Dincer and T. A. H. Ratlamwala, "Importance of exergy for analysis, improvement, design, and assessment," *Wiley Interdisciplinary Reviews: Energy and Environment*, vol. 2, no. 3, pp. 335–349, 2013.
- [46] J. Yazdanpanahi, F. Sarhaddi, and M. M. Adeli, "Experimental investigation of exergy efficiency of a solar photovoltaic thermal (PVT) water collector based on exergy losses," *Solar Energy*, vol. 118, pp. 197–208, 2015.
- [47] L. C. Ngo, *Exergetic analysis and optimization of a parabolic dish collector for low power application*, Centre for Renewable and Sustainable Energy Studies, University of Pretoria, 2013.
- [48] R. Loni, A. Kasaeian, K. Shahverdi, E. A. Asli-Ardeh, B. Ghobadian, and M. H. Ahmadi, "ANN model to predict the performance of parabolic dish collector with tubular cavity receiver," *Mechanics & Industry*, vol. 18, no. 4, p. 408, 2017.